JGR Oceans

RESEARCH ARTICLE
10.1029/2020JC016160

Nutrient-Rich Gravity Current Formed by Upwelling in Barrow Canyon: High-Resolution Observations

N. L. Beaird[1], E. L. Shroyer[2], L. W. Juranek[2], B. Hales[2], and M. A. Goñi[2]

[1]Department of Marine and Coastal Sciences, Rutgers University, New Brunswick, NJ, USA, [2]College of Earth, Ocean, and Atmospheric Sciences, Oregon State University, Corvallis, OR, USA

Abstract The distribution of nutrients influences the Chukchi Sea's rich ecosystems and affectsthe biogeochemistry of the central Arctic. Nutrients that become limiting in the late summer can be replenished episodically by physical processes that are likely to change in concert with Arctic climate trends. Here we report on unique, simultaneous, physical, and biogeochemical measurements of one such process: upwelling in Barrow Canyon. High-resolution transects of a towed vehicle, which was equipped with physical, turbulence, and biogeochemical sensors, captured the upwelling of dense, salty, and nitrate-rich waters into the shallow regions of Barrow Canyon. Upwelling drastically modifies the nitrate distribution of Barrow Canyon through the vertical advection of Atlantic Water from the Canada Basin and through turbulent flux across the nutricline. Upwelled waters form a highly sheared gravity current that is susceptible to both baroclinic and symmetric instabilities. The current exhibits transverse circulation common to frictional gravity currents. Our observations suggest that rapid and dramatic nutrient changes in Barrow Canyon can be accomplished by upwelling; the subsequent formation of unstable jets and fronts enhances the irreversible flux of upwelled nutrients to less dense waters in the Chukchi sea.

Plain Language Summary The Arctic is experiencing substantial changes, including a decline in sea ice. The Chukchi Sea is a shallow shelf that separates the Pacific from the central Arctic oceans. It has rich ecosystems, and its characteristics influence the central Arctic as waters flow from the Pacific north. In the late summer, most nutrients have been consumed in the upper layers of the Chukchi. We use an uncommon instrument to observe the details of an important oceanographic phenomena that can deliver fuel to the ecosystem in the late summer. Our instrument measures very small scale turbulence and at the same time can measure nutrients that are needed to feed the base of the ecosystem. This paper describes how deep water from the Arctic gets lifted in to the Chukchi by winds and forms a current that is unstable. Our observations allow us to measure how nutrients are impacted by this physical event.

Key Points:
- Upwelling in Barrow Canyon observed at high resolution with unique biogeochemical/turbulence platform
- Salty (34.5) nitrate-rich (14 μM) upwelled waters form dense jet susceptible to multiple instabilities
- Irreversible turbulent nitrate flux measured up to $O(1)$ mmol m^{-2} day^{-1}

Supporting Information:
- Supporting Information S1

Correspondence to:
N. L. Beaird,
nlbeaird@marine.rutgers.edu

Citation:
Beaird, N. L., Shroyer, E. L., Juranek, L. W., Hales, B., & Goñi, M. A. (2020). Nutrient-rich gravity current formed by upwelling in Barrow Canyon: High-resolution observations. *Journal of Geophysical Research: Oceans*, *125*, e2020JC016160. https://doi.org/10.1029/2020JC016160

Received 14 FEB 2020
Accepted 18 JUN 2020
Accepted article online 21 JUN 2020

1. Introduction

Arctic warming has led to a prolonged ice-free season along with a decline in sea ice concentration and thickness (Comiso, 2012; Maslanik et al., 2011; Smith, 1998). These changes, leading to increased light in the upper ocean, have the potential to significantly impact primary production and ecosystem functioning of the Arctic Ocean (Arrigo et al., 2008). The Chukchi Sea (Figure 1) forms an important gateway to the central Arctic Ocean, and its ecosystems are highly productive, supporting rich and diverse pelagic and benthic biological communities (Ashjian et al., 2010; Grebmeier, Cooper, et al., 2006). As such, changes in Chukchi ecosystems that are tied to Arctic climate trends are of significant importance.

A possible ecosystem response to observed Arctic change is enhanced primary productivity resulting from the increase in photosynthetically active radiation (PAR) that follows from the thinning and reduction in sea ice. Indeed, a few recent satellite-based studies have suggested that large increases in Arctic primary production are already underway (Arrigo & van Dijken, 2015; Kahru et al., 2016). However, depletion of nutrients from well-stratified surface waters limits growth as the ice-free season progresses. Thus, while changing light levels may alter the timing and length of seasonal phytoplankton blooms, ultimately, nutrient availability may still control growth, particularly in the late season. The net result may provide a limit on the annually integrated primary production (Arrigo, 2015; Codispoti et al., 2013). Changes in the timing, intensity, and duration of primary production can then be communicated to higher trophic levels, for example, through phasing of food availability and energy requirements or through export of carbon to benthic

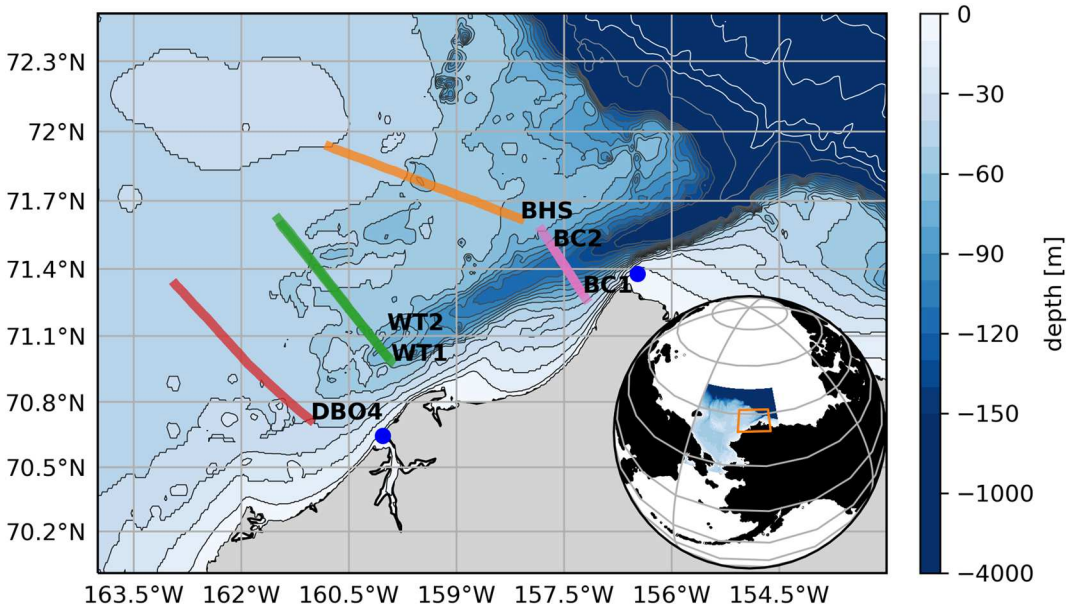

Figure 1. Sections occupied during the 2017 cruise. DBO4 = Distributed Biological Observatory Section 4; WT = Wainwright; BHS = Barrow-Hanna Shoal; BC = Barrow Canyon. Colors of each section correspond to the time periods highlighted in Figure 2. High-frequency radar sites are indicated by blue dots. The zoomed in map corresponds to the orange box shown in the inset.

communities (Grebmeier, Cooper, et al., 2006; Grebmeier, Overland, et al., 2006). As the ice-free season lengthens in the Arctic, the response of the biological pump and ecosystem will be tightly related to those physical processes capable of replenishing nutrients in the euphotic zone.

Turbulent mixing and wind-driven upwelling are prime mechanisms for episodic replenishment of near-surface nutrients. These mechanisms may change in frequency and intensity as Arctic climate changes. Nishino et al. (2015) show that episodic storms can drive vertical turbulent nitrate flux and initiate late summer/fall phytoplankton blooms in the central Chukchi. Storm activity in the Alaskan Beaufort Sea also drives upwelling on the shelf, leading to substantial shelf/basin exchange of heat, salt, nutrients, and carbon (Bourke & Paquette, 1976; Pickart, Spall, & Mathis, 2013; Pickart, Schulze, et al., 2013), influencing air-sea exchange of CO_2 (Mathis et al., 2012) and pelagic fauna distributions (Lin et al., 2016). Observations suggest that this episodic upwelling of waters from below the nutricline produces a nitrate flux capable of fulfilling the annual nitrate budget of the Alaskan Beaufort shelf over the course of four to five storm events (Pickart, Spall, & Mathis, 2013). The frequency of these upwelling favorable storms appears to have increased over the past 25 years (Pickart, Schulze, et al., 2013; Schulze & Pickart, 2012).

Biological activity is particularly strongly concentrated in Barrow Canyon (Grebmeier, Cooper, et al., 2006), a topographic depression into which many pathways of Chukchi circulation converge (Corlett & Pickart, 2017; Lin et al., 2019; Weingartner et al., 2005). Upwelling driven by winds and shelf waves is known to lift dense, nutrient-rich waters across the slope into Barrow Canyon and the Chukchi Sea (Aagaard & Roach, 1990; Ladd et al., 2016; Pickart et al., 2019; Pisareva et al., 2019; Weingartner et al., 1998; Woodgate et al., 2005). This upwelling has the potential to significantly impact the nutrient distribution of the Chukchi and Beaufort shelf (Pickart et al., 2011; Pickart, Spall, & Mathis, 2013; Pickart, Schulze, et al., 2013) and is most likely to occur when the Beaufort High is strong and the Aleutian low deep (Pisareva et al., 2019).

The mean flow in Barrow Canyon is downcanyon, toward the Arctic, with depth averaged speeds of 10 to 20 cm s^{-1} (Weingartner et al., 2017). Upcanyon reversals of the flow happen about 30% of the time and are associated with stronger velocities (Weingartner et al., 2017). Circulation in the canyon exhibits seasonality with strong downcanyon flow in summer; weaker, and more variable, upcanyon flow in fall; and negligible winter transport (Weingartner et al., 2017). Upwelling events that cause reversals to upcanyon flow can either return Pacific-origin Winter Water that has already traversed the Chukchi or raise

Atlantic-origin water from the Canada Basin. Both water masses are nutrient rich and thus have the potential to fuel biological production. At the Alaskan Beaufort shelf, Lin et al. (2019) show that two thirds of upwelling events bring Atlantic-origin Water and one third Pacific-origin Water, with Atlantic Water upwelling events connected to a seasonal cycle in Atlantic Water/Pacific Water interface depth and less common in summer. However, in the Chukchi at the head of Barrow Canyon (further from the shelf break), Pisareva et al. (2019) show that upwelling tends to return Pacific Winter Water to the canyon and that Atlantic Water upwelling appears to be more rare.

The focus of this study is physical mechanisms that are capable of bringing nutrients into the depleted surface waters of the Barrow Canyon of the Chukchi Sea. We report on novel high-resolution, simultaneous, physical, and biogeochemical observations of an upwelling event in Barrow Canyon. The upwelling event substantially modifies the nutrient distribution in Barrow Canyon, both via advection of nutrient-rich water masses and by apparent instability that increases mixing and stirring of the water column. The data and processing methods are outlined in section 2. Observations of the upwelling event in Barrow Canyon are presented in section 3. The dynamics of the current formed by upwelling, including its turbulence and stability properties, is discussed in section 4. Impacts on the nutrient distribution in Barrow Canyon are presented in section 5.

2. Data and Methods

Coincident observations of the physical state, including turbulent microstructure, and nutrient concentrations were made from a towed platform known as the SuperSucker (Hales, Moum, et al., 2005; Hales, Takahashi, & Bandstra, 2005). Instruments deployed with the towed platform, and analyses of the water pumped back from it, are the primary sources of data. These data are supplemented with meteorological and radar data from coastal stations, as well as and shipboard velocity data.

The towed platform enables unique observations of physical and biogeochemical features that have been shown to have important variability on length scales smaller than resolution achieved by most shipboard surveys in the region (Martini et al., 2016; Timmermans & Winsor, 2013). Martini et al. (2016) describe biogeochemical variability on scales down to 150 m, while Timmermans and Winsor (2013) establish the presence of horizontal density variance down to $\mathcal{O}$(1 km) submesoscales, approximately the internal Rossby radius for the surface layer. The Rossby radius based on pycnocline stratification during the cruise was $\mathcal{O}$(10 km) (calculated from $\lambda = \frac{NH}{f}$ using an average stratification of $N^2 = 0.2 \times 10^{-3}$ s^{-2} and H as the water depth).

The cruise took place from 7 to 22 August 2017 aboard the R/V *Sikuliaq*. Four sections were occupied in the northeastern Chukchi Sea, including some survey lines of the Distributed Biological Observatory (DBO) (Moore & Grebmeier, 2018) (Figure 1): the Distributed Biological Observatory Section 4 (DBO4), Wainwright section (WT), Barrow-Hanna Shoal section (BHS), and Barrow Canyon section (BC, also known as DBO5). Each section was occupied at least twice: once with "coarse"-resolution CTD sampling, immediately followed or preceded by high-resolution SuperSucker sampling. Two sections (Wainwright and Barrow Canyon) were reoccupied, resulting in two CTD and two SuperSucker occupations each, referred to here as WT1/WT2 and BC1/BC2. Here, we focus on the repeated occupation of the Barrow Canyon section before and after an upwelling event. Due to pressure-induced sensor malfunction, the SuperSucker was limited to the upper 50 m during BC2, and thus, the deeper portion of the canyon was not measured. Other sections will be the focus of another study as they were not directly influenced by the upwelled waters that are the subject of this manuscript.

2.1. SuperSucker Towed Vehicle

The SuperSucker is a towed profiling vehicle capable of pumping water samples ship board for real-time analyses (Hales, Moum, et al., 2005; Hales, Takahashi, & Bandstra, 2005). This winch-controlled profiler makes specified depth versus time profiles, producing a sawtooth patterned vertical section when towed behind a moving ship. The vehicle can profile at vertical speeds of 0.05–0.5 m s^{-1} while being towed at 0 to 1.5 m s^{-1} horizontally. The horizontal and vertical resolutions of the profiles depend on user-targeted vertical and horizontal speeds and sensor sampling rate. The horizontal resolution varies with depth and is a

function of ship speed and total water depth or depth/altitude limits set by the operator. For the Barrow Canyon sections, the horizontal resolution at middepth is roughly 600 m for BC1 and 300 m for BC2. Vertical resolution of the raw data varies with sensor sampling rate (from 100 Hz for microstructure to 0.14 Hz for the nutrients) and vertical velocity (about 0.1 m s^{-1}). However, all observations are binned to 1 m in the vertical.

The vehicle carries in situ sensors including a SeaBird 9+ CTD with dual temperature and conductivity sensors, as well as optical sensors to measure backscatter, PAR, chlorophyll fluorescence (Chl-Fl), and colored dissolved organic matter (CDOM). In addition, a pump intake located near the in situ sensors carries seawater along the tow cable to the ship for continuous analysis of inorganic nutrients (NO_3, P, and Si) and inorganic carbon (pCO_2 and DIC). We focus here on the NO_3 measurements and note that the pumping and shipboard analyzer have a response time of about 15 s, which acts to low-pass filter the nitrate signal. The vertical profiling speed and the response time together act to smooth nitrate gradients at 1.5 to 3 m scales. This will tend to underestimate the nitrate gradients and therefore produce underestimates of the turbulent nitrate flux.

A 500 kHz RDI Sentinel V50 Acoustic Doppler Current profiler was mounted to the SuperSucker to measure water velocity. A process similar to the shear method outlined in Fischer and Visbeck (1993) was used to remove platform motion and obtain absolute velocity from the SuperSucker-mounted 500 kHz ADCP. First, shear estimates were produced by rotating single-ping data into earth coordinates, matching depth cells, and taking the vertical derivative to remove platform motion. All shear profiles in a single ascent or decent of the SuperSucker were averaged into 1 m depth bins. The root mean squared error of the SuperSucker shear relative to the shipboard ADCP was 0.6 cm s^{-1} m^{-1}. Both instruments independently measure the shear bands apparent in the flow (see Figure S1 in the supporting information). Profiles of relative velocity were created by vertically integrating the average shear. These baroclinic, or relative, velocities match the baroclinic component of the shipboard ADCP well, with an root mean squared error or 5 cm s^{-1} (see Figure S2). Finally, absolute velocity profiles were calculated by setting the depth mean of the SuperSucker relative velocity equal to the depth mean of overlapping bins from the ship-mounted 150 kHz ADCP. Rough estimates of vertical velocity are found following methods in Thurnherr (2011): The time derivative of depth is subtracted from the ADCP measured vertical speed, and then the remaining vertical speed is averaged in depth and time bins.

2.2. GusT Temperature Microstructure

Observations of turbulent microstructure were obtained via GusT instruments mounted on the leading edge of the SuperSucker. GusTs are self-contained packages integrating a fast FP07 thermistor, three-component accelerometer, compass, pressure sensor, and pitot tube (Moum, 2015). All sensors are sampled at 100 Hz with the exception of the compass (4 Hz). The GusT is similar to the χpod (Moum & Nash, 2009) with smaller form factor, battery pack, and sensor load for shorter deployments. Temperature microstructure was used to calculate the rate of dissipation of temperature variance (χ_T) and the turbulent temperature diffusivity (K_T) following Moum and Nash (2009).

Estimates of χ_T are obtained by fitting the spectrum of the measured horizontal temperature gradient to a theoretical spectrum (Batchelor, 1959) over a finite bandwidth, taken here to be the viscous-convective subrange. The method requires assumption of a mixing efficiency. We used a value of 0.2 (Gregg et al., 2018) and limit calculation of turbulence quantities to stably stratified conditions. The method also depends on conversion from a frequency to wave number spectra and so relies on known flow speed past the sensor and Taylor's frozen flow hypothesis (Taylor, 1935). Flow speed past the sensor is known from the vehicle-mounted Doppler profiler. We estimate K_T and χ_T following Osborn and Cox (1972) and Osborn (1980) using methods detailed in Moum and Nash (2009).

2.3. Meteorological and High-Frequency Radar Time Series

Wind speed and direction were obtained from the Pt. Barrow observatory in Utqiaġvik, Alaska. The data were accessed via the National Climate Data Center of the National Oceanic and Atmospheric Administration (http://www.ncdc.noaa.gov/).

Surface currents were obtained from high-frequency radar observations collected at coastal stations (Fang et al., 2017). Radar data are provided by the U.S. Integrated Ocean Observing System (IOOS) High Frequency Radar Network (HFRNet) and accessed through the Coastal Observing R&D Center (CORDC).

3. Observations of Upwelling in Barrow Canyon

During the 2017 cruise reported here, an upwelling event brought nutrient-rich Atlantic Water ($S > 33.6$) to the surface in Barrow Canyon. Winds were out of the northeast, blowing in the upwelling favorable direction, for a period of 3 days between 12 and 15 August 2017 (Figure 2). Wind speed exceeded 6.5 m s^{-1} for more than a day, meeting the upwelling criteria suggested by Pickart et al. (2019), who, using 24 repeat occupations of the DBO5 (our Barrow Canyon) line, find the best correlation between the presence of upwelled dense water and upcanyon winds along 52°T. They suggest a threshold for wind-driven upwelling in Barrow Canyon when the upcanyon (52°T) wind speed exceeds 6.5 m s^{-1} for at least 20 hr. Using high-frequency radar data, Fang et al. (2017) show that the surface currents in the area reverse when local winds are northwesterly at speeds exceeding 6 m s^{-1}. In 2017 the ship was not in Barrow Canyon during the upwelling period, but shore-based high-frequency radar observations showed a current reversal to upcanyon flow (Figure 2), demonstrating the oceanic upwelling response to the winds. Occupations of the Barrow Canyon line before and after upwelling winds show extensive changes in the nutrient distribution and hydrographic structure in response to the wind event (Figures 3 and 4).

The first occupation of the section on 9–10 August (BC1, Figures 3a, 3c, and 3e), before upwelling, resembled the climatological mean state described by Pickart et al. (2019). Warm Alaskan Coastal Water was found on the onshore slope of the canyon (Figures 3a and 4a). Around 20–25 km from shore light and dense isopycnals diverge in the vertical, creating a density front and a maximum in downcanyon velocity. Around 25 km offshore, a strong temperature front was present above and below the 1,025.20 kg m^{-3} isopycnal. Offshore of this temperature front cold Remnant Winter Water, high in nutrients (≈10 μM Lowry et al., 2015), was found at depth (Figures 3c and 4a). Above the Remnant Winter Water, a layer of Bering Summer Water was found, and above that a layer of modified Melt Water (Figure 4a). Nutrients were completely depleted in the upper 40 m of the water column before the upwelling event. Water masses are defined here following the descriptions in Pickart et al. (2019), who note that these definitions are only approximate due to significant variability in endmember hydrographic properties.

We adopt a canyon-referenced coordinate system with downcanyon (y) flow positive to the northeast, toward the Canada Basin, and cross-canyon (x) positive toward shore. Flow in BC1 was downcanyon nearly everywhere, with the highest speeds at the onshore side of the section. Very weak upcanyon flow was found at depth at the offshore end of the section (Figure 3e).

Six days later, and approximately 12 hr after the cessation of upwelling favorable winds, the Barrow Canyon section was reoccupied (BC2, 16 August). A substantially altered water column structure was observed (Figures 3b, 3d, and 3f). In BC2 dense, salty, nutrient-rich, Atlantic Water upwelled from the Canada Basin was present over the onshore slope of the canyon, while the warm, fresh, Alaskan Coastal Water was compressed into the surface layer and advected offshore (Figures 3b and 4b). All isopycnals present in BC1, as well as many denser surfaces, outcropped above the onshore slope of the canyon. Stratification increased dramatically in this region, and the density of the lower layer increased from 1,025.9 to 1,027.7 kg m^{-3} as salinity increased to 34.5.

Nitrate concentrations in the upper 50 m over the onshore side of the canyon increased from 0 to 14 μM between the two occupations. The highest nitrate concentrations of the cruise were found in this upwelled Atlantic Water, exceeding even the nutrient-rich Remnant Winter Water present in BC1 (Figures 3d and 4). In addition to the increase in nitrate due to lifting of Atlantic Water isopycnals, nitrate concentrations of less dense waters also increased. These changes can be seen in nitrate differences in temperature salinity bins (Figure 4c) and reflect a diapycnal nutrient flux.

While hydrographic conditions showed the result of upwelling, the second Barrow Canyon transect occurred after upwelling favorable wind forcing had ceased (Figure 2). The circulation in the canyon during BC2 was largely downcanyon with a small core of upcanyon flow above the nutrient-rich Atlantic Water

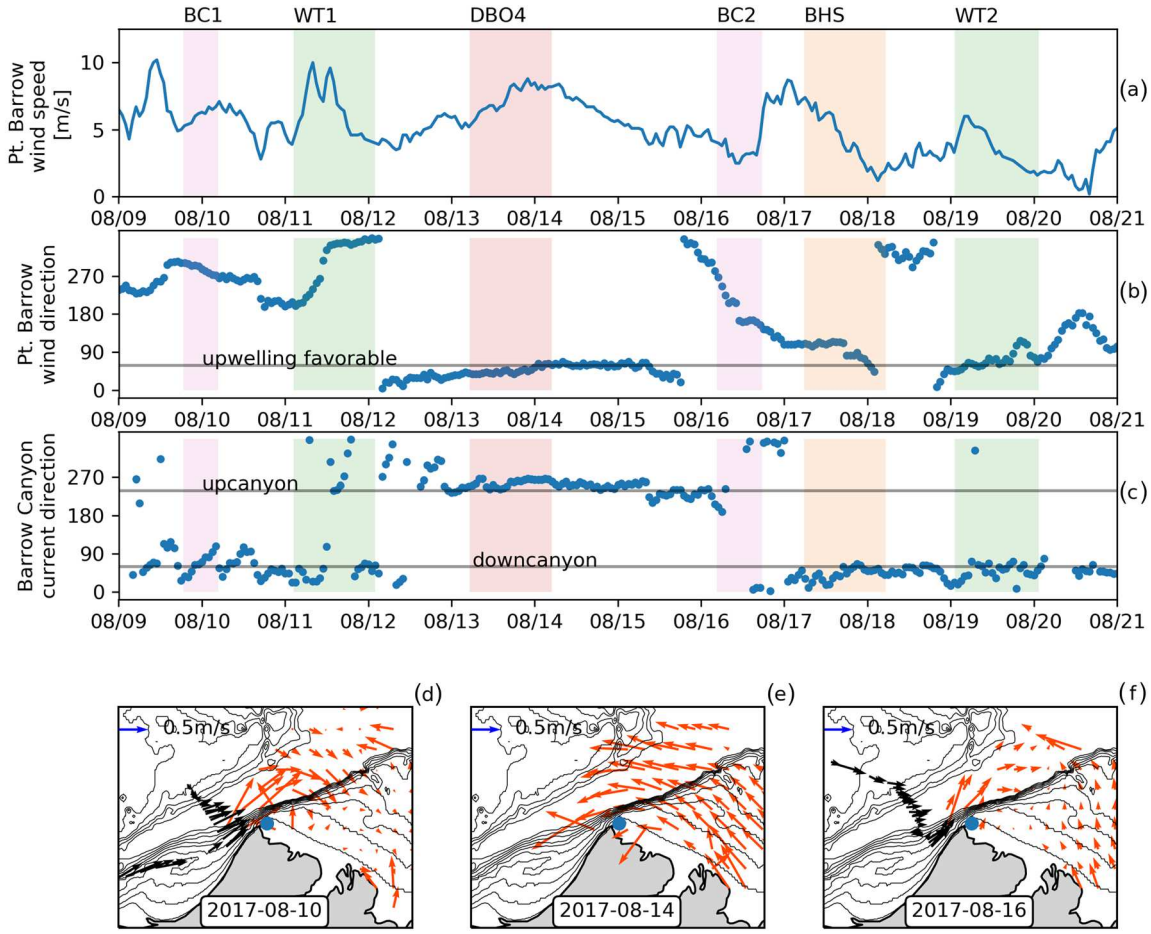

Figure 2. Time series of Point Barrow wind speed (a), wind direction (b), and HF radar surface current direction in the Barrow Canyon region (c). HF radar surface currents before (d), during (e), and after (f) upwelling shown in the bottom three maps. In a–c, upcanyon and downcanyon directions are indicated, as is the upwelling favorable wind direction (52°T). The time of each SuperSucker section is indicated in color matching the sections in Figure 1. In d–f, Barrow Canyon surface currents are obtained from the shallowest shipboard ADCP bin (black) and from high-frequency radar observations (red, radar sites shown as blue dots).

(Figure 3f). The upwelled Atlantic Water was situated in a strongly sheared jet that flowed downcanyon, draining upwelled waters back into the deep Canada Basin (Figure 5a).

Though very dense water was upwelled, the wind forcing preceding BC2 was not particularly strong. This is consistent with a variety of studies that find little correlation between the strength or duration of the regional upwelling winds and the type of water upwelled into Barrow Canyon (Li et al., 2019; Pickart et al., 2019; Weingartner et al., 2017). Though Lin et al. (2016) show that the presence of Atlantic Water in nearby Alaskan Beaufort Sea is dependent on the windstress curl through its control of the Atlantic Water interface height. The hydrographic structure observed along BC2 is consistent with the climatological upwelling state described in Pickart et al. (2019), though the extent of the upwelled Atlantic Water may be anomalous. The upwelling observed here raises isopycnals from fairly deep (approximately 250 m for the 34.5 isohaline Pickart, 2004) in the Canada Basin to the surface in Barrow Canyon.

In addition to the newly upwelled Atlantic Water in BC2, significant stirring and redistribution of other water masses are apparent. Much shorter length-scale features were observed in BC2 than in BC1, particularly over the deep portion of the canyon. These features can best be seen as small scale ($\mathcal{O}$(1 km)) bands in the temperature distribution (Figure 3b). This enhanced high wave number horizontal temperature variance along isopycnals in BC2 relative to BC1 is perhaps a consequence of increased flow instability. Variability on these small scales has been observed by previous high-resolution surveys in

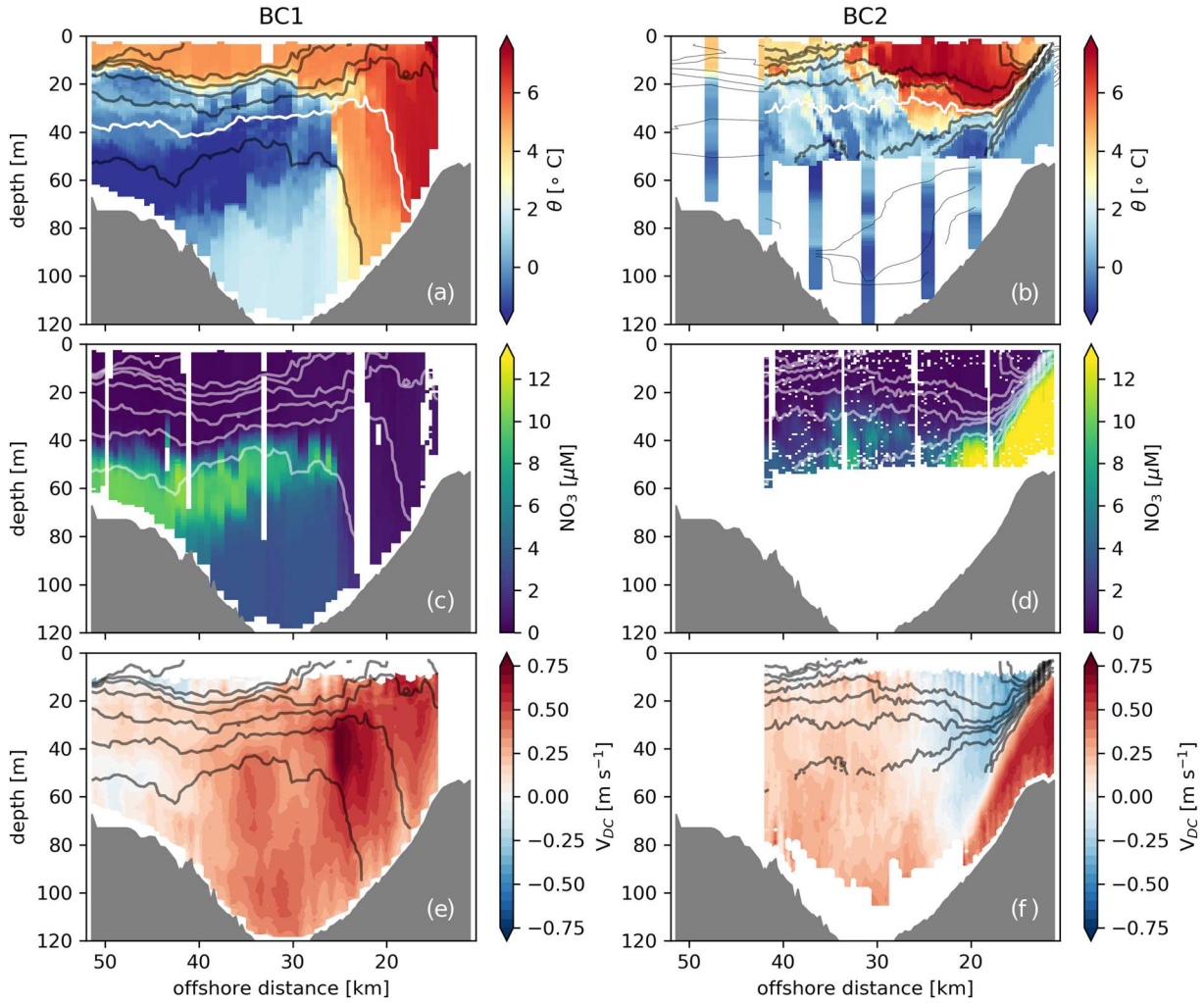

Figure 3. First (a, c, e) and second (b, d, f) occupations of a section across Barrow Canyon. Potential temperature (a, b), Nitrate (c, d), and velocity in the downcanyon direction (e, f). Potential density (1,023.3 to 1,027.7 kg m^{-3}, every 0.4 kg m^{-3}) is contoured in each panel; in a and b, the 1,025.20 kg m^{-3} contour is highlighted in white. Potential temperature (color) and potential density (contours) from the CTD section subsequent to the SuperSucker section are shown in b.

the Chukchi (Martini et al., 2016; Timmermans & Winsor, 2013; Weingartner et al., 2013). The structure, potential vorticity, and possible mechanisms of instability of the nutrient-rich jet are discussed in the next section.

4. Dynamic Structure of Outflow

The dominant feature of the post-upwelling BC2 section is the jet encompassing the dense, nutrient-rich, Atlantic Water draped over the onshore slope of the canyon (Figure 5a). This jet likely formed when the upwelling favorable wind forcing stopped and the uplifted dense waters adjusted to form a dense outflow reminiscent of a gravity current.

The nutrient-rich current covered the onshore slope of Barrow Canyon. It was bounded by a sharp front, across which vorticity, vertical shear, stratification, and lateral density gradients were very strong (Figure 5). Within the front relative vorticity, ζ, exceeded f, with Rossby number, $R_o=\zeta/f>3$ (Figure 5c). Additionally, the isopycnal slope of the front was steep relative to N/f, which is expressed by the balanced Richardson number, $Ri_b=\frac{f^2N^2}{M^4}<1$, where $M^2=\frac{g}{\rho_o}\frac{\partial\rho}{\partial x}$ (Figure 5d). The order one R_o indicates that both rotation

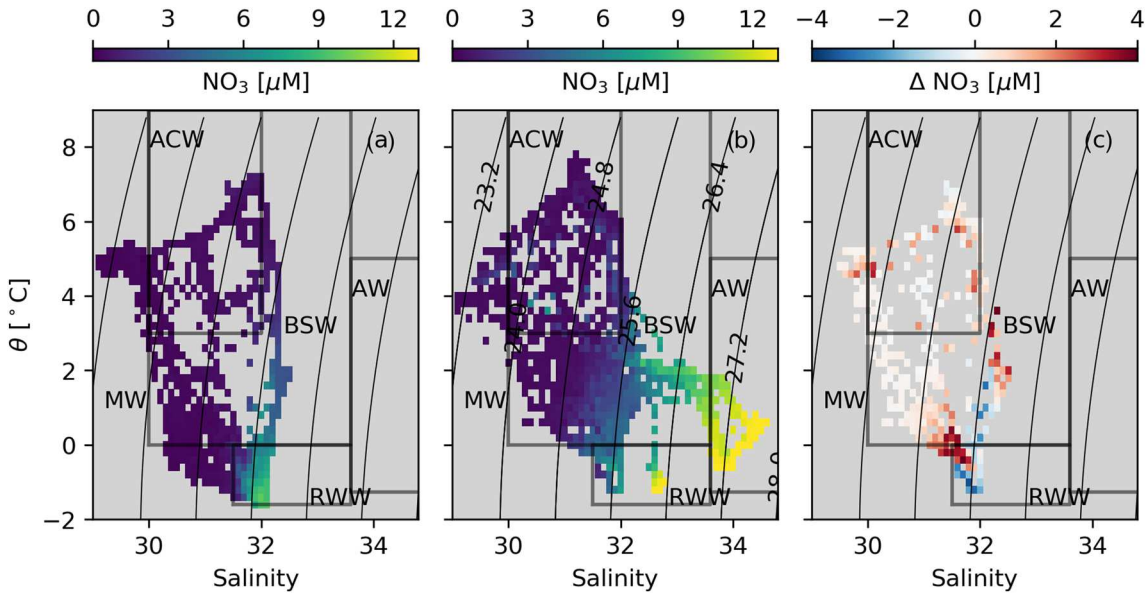

Figure 4. Nitrate in temperature salinity space on BC1 (a), BC2 (b), and the difference between the two (c). Water mass definitions as outlined in Pickart et al. (2019): AW = Atlantic Water; RWW = Remnant Winter Water; BSW = Bering Summer Water; ACW = Alaskan Coastal Water; MW = modified meltwater/runoff. Potential density anomaly is contoured in black.

and inertia are important to the flow. The small balanced Richardson number indicates that horizontal buoyancy gradients are strong relative to the vertical buoyancy gradients. Together, these scalings, $\mathcal{O}(1)$ R_o and $\mathcal{O}(1)$ Ri_b, suggest that the jet may be influenced by submesoscale dynamics and symmetric instability (Thomas et al., 2008). These dynamics are characterized by enhanced ageostrophic vertical velocities that may have important impacts on biology (Mahadevan, 2016) and by a forward cascade of energy that transfers energy to smaller scales where mixing occurs (Thomas et al., 2013).

A transverse secondary circulation was apparent in the gravity current with onshore flow in the jet core and interface and offshore flow in a bottom boundary layer (Figure 5b). A parcel of water within the gravity current moves in a spiral, or helical, pattern as it flows downstream, moving from the upper interface of the flow to the bottom boundary as it flows downstream (see, e.g., Figure 11a in Darelius, 2008). This secondary circulation is a common feature observed in rotating gravity currents and may enhance interfacial mixing (Darelius, 2008; Fer et al., 2010; Johnson & Ohlsen, 1994; Umlauf & Arneborg, 2009). Johnson and Ohlsen (1994) suggest these transverse secondary circulations form due to transport to the left of the along-stream flow in both a bottom Ekman layer and in an Ekman layer at the density interface capping the jet. The convergence of the two Ekman layers is compensated by flow to the right of the jet in the interior. Later studies describe the transverse dynamics as the balance of the along-stream tilt in the density interface with a cross stream geostrophic flow (Umlauf et al., 2010; Wåhlin, 2004). An ageostrophic secondary circulation of different origin in Barrow Canyon has been investigated before and has been shown to influence canyon circulation (Signorini et al., 1997).

Rough estimates of vertical velocity obtained from the SuperSucker-mounted ADCP (not shown) hint at positive vertical velocity (as large as 3 cm s^{-1}) associated with the layer of onshore flow and the tilt of isopycnals. However, this estimate may be strongly affected by small biases in tilt or roll of the ADCP. For comparison, a vertical velocity of 1 mm s^{-1} is inferred from the measured onshore flow speeds (~0.1 m s^{-1}; Figure 5b) and isopycnal slope (~10 m km^{-1}). This second estimate is remarkably similar to that calculated based on the divergence of the radar velocity (see Figure S3). Radar data indicate a region of surface divergence (0.1 m s^{-1} km^{-1}) on the shoreward end of the BC2 transect. Using an upper layer depth of roughly 10 m, this surface divergence converts to an upwelling vertical velocity of approximately 1 mm s^{-1}. These more conservative estimates of vertical velocity at the front are still very strong (85 m day^{-1}), emphasizing the importance of the submesoscale in vertical exchange.

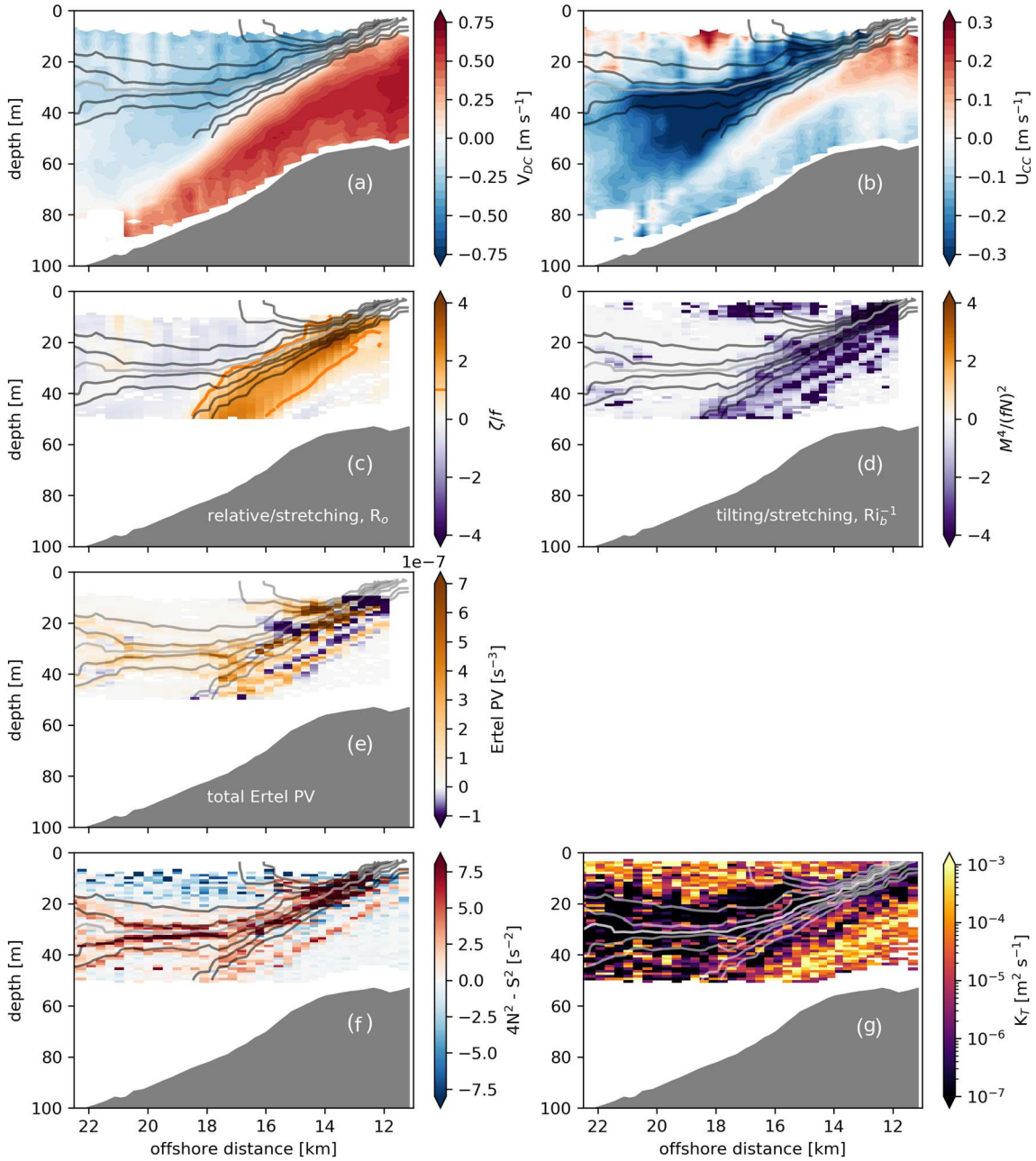

Figure 5. The onshore slope of Barrow Canyon during the second occupation (BC2). (a) Downcanyon speed (positive downcanyon), (b) cross-canyon speed (positive onshore), (c) the relative vorticity scaled by the stretching term (equivalent to the Rossby number) with R_o=1 as a solid contour, (d) the tilting term of the Ertel potential vorticity relative to the stretching term (equivalent to the inverse balanced Richardson number), (e) the total Ertel potential vorticity, (f) reduced shear, and (g) turbulent diffusivity.

4.1. Current Instability and Lateral Stirring

To evaluate the stability and dynamics of the nutrient-rich current, we calculate the Ertel potential vorticity (q), defined as

$$q = (f\hat{k} + \nabla \times \mathbf{u}) \cdot \nabla \mathbf{b}, \tag{1}$$

where f is the Coriolis parameter, $\hat{k}$ is the vertical unit vector, $\mathbf{u}$ is the velocity vector, and the buoyancy is $\mathbf{b} = -g\rho/\rho_o$. We define an along-canyon coordinate system with y positive downcanyon toward the

Canada Basin, and x positive cross-canyon toward shore. Velocity is rotated into downcanyon (v) and cross-canyon (u) components. Within Barrow Canyon, cross-canyon changes in along-canyon velocity dominate the relative vorticity ($\partial v/\partial x \ll \partial u/\partial y$), so we make the approximation that $\zeta = \nabla \times \mathbf{u} = \partial v/\partial x$. We also assume $\partial v/\partial z \times \partial b/\partial x \gg \partial u/\partial z \times \partial b/\partial y$, which should be true of nearly geostrophic flows like this one, and arrive at the approximation

$$q \approx (f + \zeta)N^2 + \frac{\partial v}{\partial z}M^2. \tag{2}$$

We further assume thermal wind balance holds such that $\partial v/\partial z = -\frac{1}{f}M^2$, giving an expression for the Ertel potential vorticity

$$q \approx \underbrace{fN^2}_{stretching} + \underbrace{\zeta N^2}_{relative} - \underbrace{f^{-1}M^4}_{baroclinic}, \tag{3}$$

which has three vorticity terms: stretching (planetary), relative, and baroclinic (tilting).

A variety of overturning instabilities may be present in regions of a flow where the Ertel potential vorticity becomes negative, $q < 0$ (Hoskins, 1974; Thomas et al., 2008). The relative role of each of the three terms in driving q below zero allows us to assess the type of potential instabilities of the flow. In our observations the stretching term is positive and dominates q outside the gravity current. Within the front formed by the gravity current, the relative and baroclinic vorticity terms begin to dominate over the stretching PV (Figures 5e and 5f). The relative vorticity is uniformly positive across the front, which increases the total q. Despite the strong cyclonic relative vorticity ($\zeta > 0$), q can still drop below zero as the baroclinic term is negative definite and always acts to reduce the PV of the fluid (Thomas et al., 2013). Above the nutrient-rich jet, the baroclinic term of the potential vorticity is large and negative, of the same order as ζN^2, and several times larger than fN^2 (Figure 5e). Thus, within the front, q is occasionally negative and therefore susceptible to dynamic instabilities (Figure 5e).

The type of instability can be determined by considering an alternate form of the potential vorticity instability criteria (Thomas et al., 2013). The negative Ertel potential vorticity instability criteria may be written as $\varphi_{Ri_B} < \varphi_c$, where φ_{Ri_B} is the balanced Richardson number angle $\varphi_{Ri_B} = tan^{-1}(-N^{-2}|v_z|^2)$ (also, $\varphi_{Ri_B} \approx tan^{-1}((fN)^{-2}M^4)$) and φ_c is a critical angle $\varphi_c \approx tan^{-1}(-1 - f^{-1}v_x)$ (Thomas et al., 2013). The value of φ_{Ri_B} indicates whether the flow is susceptible to gravitational, inertial, or symmetric instability (Thomas et al., 2013).

Values of φ_{Ri_B} (not shown) calculated for the BC2 section indicate that regions of the flow are conducive to symmetric instability within the bands where $q<0$ (Figure 5g). Symmetric instability is an instability that derives its energy from the geostrophic shear of the fluid and gives rise to "slantwise" convection with enhanced vertical velocities and increased shear. Symmetric instability has been hypothesized as a source of enhanced vertical nutrient flux feeding primary production in oceanic fronts (Brannigan, 2016; Mahadevan, 2016). These mechanisms have also recently been shown to enhance mixing and exchange between gravity currents and interior waters along steep topography (Naveira-Garabato et al., 2019) and other bottom boundary layers (Wenegrat & Thomas, 2020).

Baroclinic instability, which develops more slowly than the submesoscale instability outlined above, may also act to enhance stirring of the nutrient-rich gravity current with nutrient-poor waters offshore. A necessary condition for the growth of baroclinic instability is a change in sign of the horizontal potential vorticity gradient across the flow. The broad-scale potential vorticity gradient changes from $\partial q/\partial x > 0$ offshore of the front to $\partial q/\partial x < 0$ onshore of the front and has many more sign changes on small scales. This suggests that the flow also may be baroclinically unstable and capable of shedding eddies.

Another region of negative potential vorticity and mechanism of eddy formation is likely to exist closer to shore where frictional torque should act to reduce the downcanyon speed, creating anticyclonic relative vorticity (D'Asaro, 1988). This region is closer to shore than our section extends, so it is not apparent in our observations. A conservative estimate of the anticyclonic relative vorticity assumes the downcanyon flow goes to zero linearly between our section and the coast: $\zeta \approx \frac{-0.75 m/s}{10.5 km} \approx -0.5f$.

Thus, we find that the flow is susceptible to both slower (baroclinic) and rapid (symmetric) mechanisms of instability that can lead to mixing and stirring of the high-nutrient dense gravity current and ambient waters. These mechanisms may explain the observed increase in small-scale variability in the hydrographic properties during BC2 (Figure 3b). These instabilities may play a role in the irreversible transfer of nutrients into adjacent nutrient-depleted regions of the upper water column.

4.2. Diapycnal Mixing

The interface above the jet was strongly stratified, tending to suppress turbulence. However, the vertical shear was also very large, and in some regions the reduced shear, $4N^2 - \frac{\partial u^2}{\partial z}$, dropped below zero (equivalent to Richardson number, N^2/S^2, less than the critical value of 1/4) (Figure 5f). In these bands shear-driven instabilities have the potential to grow and induce diapycnal mixing. Bands of negative-reduced shear are present within the jet interface and core and correspond to regions of increased turbulent diffusivity of up to $\mathcal{O}(10^{-3})$ $m^2\ s^{-1}$ (Figure 5f and 5g). These elevated diffusivities are consistent with previous observations of enhanced turbulent dissipation in Barrow Canyon (Shroyer, 2012).

By increasing shear and connecting boundary and interior regions of the jet, the transverse flow provides an additional mechanism for shear-driven mixing and vertical circulation (Fer et al., 2010; Johnson & Ohlsen, 1994; Naveira-Garabato et al., 2019; Umlauf et al., 2010). Additionally, the secondary circulation adds to cross-shore transport. Thus, it may play a role in mixing waters between the gravity current and the ambient waters, contributing to irreversible flux of nutrients.

5. Impact on Nutrients

The upwelling event observed here is one example of an episodic physical process that may drive late summer biological growth in the Chukchi. It significantly increased upper water column nutrient concentrations through the advection of the deep Canada Basin nutricline (Atlantic Water) and through mixing and stirring. Lowry et al. (2015) show that chlorophyll and phytoplankton biomass in the surface waters of the Chukchi are strongly correlated with the presence of high-nutrient water masses like Remnant Winter Water or the Atlantic Water present in Barrow Canyon post upwelling. Thus, processes, like upwelling, that impact the nutrient distribution are likely to have an effect on the Chukchi ecosystem in the nutrient-limited late summer. The simultaneous physical-biogeochemical observations of the SuperSucker allow us to describe the dynamics and impacts of the event on distributions of growth-limiting nitrate.

Nitrate concentrations at common depths differed between the two occupations by as much as 14 μM. By far the largest changes were due to vertical heaving of isopycnals, lifting Atlantic Water into the canyon where it had not been present before, and increasing the nitrate concentrations above the onshore slope of the canyon (Figures 3c and 3d). However, part of the change occurs within water masses present in both occupations. The role of vertical advection and turbulent diffusivity in changing the nitrate distribution between sections is discussed next.

5.1. Vertical Nitrate Advection

The nitrate difference between BC1 and BC2 is largest above the onshore slope of the canyon (Figures 3c and 3d) and is largely due to the vertical movement of Atlantic Water. This advection is the result of the vertical component of the upwelling circulation.

A simple estimate of the advective component of the upward nitrate flux can be made by multiplying the Atlantic Water nitrate concentration ($C^{AW}_{no_3}$) by the upwelling velocity (w_u):

$$J_{upwelling} = w_u * C^{AW}_{no_3}. \tag{4}$$

A rough estimate of the upwelling velocity (~50 m/day) can be made using the displacement of the 34 isohaline and the observed duration of upwelling winds (~3 days). Here, the displacement was approximated as ~150 m, based on the observed signal in BC2 and the climatological level of the 34 isohaline on the Beaufort slope (180 m; Pickart, 2004). Uncertainty around the initial depth of the 34 isohaline strongly influences this estimate, and the magnitude of the estimated upwelling using the climatological level points toward other processes (e.g., slope waves) amplifying upwelling. A more conservative estimate can be made by

assuming that the total offshore Ekman transport (taken simply to be the along-shore windstress divided by density times the Coriolis parameter: $\tau/\rho f$) is replaced by vertical velocity (w_u) acting over the width of the Rossby radius (λ) (Garvine, 1971), such that

$$w_u = \frac{\tau}{\rho f \lambda}. \quad (5)$$

Using a value of 7 m s^{-1} for the wind speed (Figure 2) and a Rossby radius of λ=10 km (calculated from $\lambda = \frac{NH}{\pi f}$) in Equation 5 gives an upwelling speed of about 5 m day^{-1}. Assuming an Atlantic Water nitrate concentration of 14 μM, Equations 4 and 5 give a vertical advective nitrate flux of 70 mmol m^{-2} day^{-1}. It should be noted that this large vertical flux is reversible; that is, these nutrient-rich isopycnals could relax back to their neutral depths (~180–250 m Pickart, 2004) after upwelling winds stop and before the nitrate can be fully consumed. Recall that the instantaneous advective fluxes at the front would be 10 times stronger than those summarized above which were inferred from the upwelling wind stress (vertical velocities of ~1 mm s^{-1} are inferred based on the isopycnal slope and radar velocity). This contrast emphasizes the significance of small scales (submesoscale) in vertical transport (Mahadevan, 2016).

This estimate of the advective nitrate flux is larger than previous regional estimates of upwelling flux made by Pickart, Schulze, et al. (2013) on the Beaufort Shelf. Pickart, Schulze, et al. (2013) used a density-nitraterelationship established from cruise data to estimate nitrate upwelling from moored instruments. They find the nitrate flux to be 16 mmol m^{-2} day^{-1} averaged across seven storms. To use comparable units, we took the average cumulative nitrate flux of 61 mmol m^{-2} per storm reported by Pickart, Schulze, et al. (2013) and divided by their average storm duration of 3.8 days. Our estimate appears to be larger due to higher nitrate concentrations in our Barrow Canyon observations, rather than differences in the vertical velocity estimates. We estimate upwelling velocities (5 m day^{-1}) that are actually significantly lower than those estimated by Pickart, Schulze, et al. (2013) (20 m day^{-1}). It should be noted that our estimate is based on an approximate calculation while the Pickart, Schulze, et al. (2013) estimate is based on observations that resolve the time evolution of upwelling events.

As will be shown in the next section, the advective flux is much larger than the associated turbulent nitrate flux. However, the smaller turbulent flux is critical to transferring nutrients across density surfaces into the lighter waters that permanently reside in or near the euphotic zone.

5.2. Turbulent Nitrate Flux

The vertical advection of Atlantic Water brings nutrients to the surface, but it is possible for these dense waters to relax to their former depth before significant biological consumption can occur. To fuel new production, either the nutrient-rich waters must remain lifted into the euphotic zone for a sufficient time to be used or mixing must transfer nutrients across density interfaces (down gradient) into less dense layers that permanently reside near the surface. The flavors of instability that affect the nutrient-rich jet may facilitate the diapycnal mixing required to transfer nutrients to shallower waters.

To investigate the irreversible nutrient flux, we calculate turbulent fluxes using the GusT microstructure data and compute the change of nutrient distribution within temperature-salinity bins. Using a water mass framework (differences calculated in temperature-salinity space rather than depth-distance coordinates) minimizes the changes directly due to advection of new water masses (like Atlantic Water) and highlights changes due to mixing among water masses present in both occupations. We assume here that changes within temperature-salinity bins are due to turbulent flux. However, we note the caveat that this analysis could be confounded by the advection of a single water mass with a spatial gradient in nitrate. Comparison of the independent calculations of turbulent flux and nitrate changes in temperature-salinity space will provide one check on this assumption. Nitrate differences calculated in temperature-salinity bins (as in Figure 4c) can be transformed back into physical space to produce a cross-canyon section of nitrate change within water masses (Figure 6). This framework only produces observations of nitrate change in regions where the water mass properties were shared between BC1 and BC2. We see that nitrate increased in some water masses (up to 4 μM) and decreased in others (Figure 6).

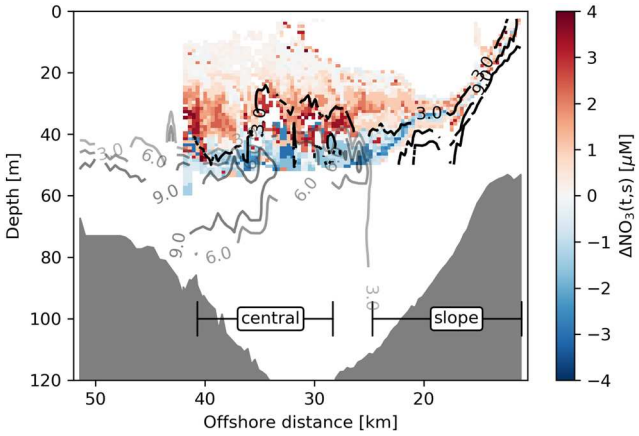

Figure 6. Difference in nitrate between BC1 and BC2 calculated in temperature-salinity bins as in Figure 4c and mapped onto the corresponding temperature-salinity values in in the second Barrow Canyon occupation. Values are only shown for overlapping temperature-salinity properties between the two sections; thus, the upwelled Atlantic Water is not shown in the difference plot. Contours of nitrate concentration from BC1 (gray) and BC2 (black).

We consider two regions when describing the evolution of the nutrient distribution in Barrow Canyon: The "slope" region comprises the onshore slope of the canyon where the nutrient-rich gravity current is found; the "central" region covers the deep part of the canyon, offshore of the gravity current (Figure 6). The two regions are roughly divided by the dominant nitrate source, with Atlantic Water being the main source on the slope, and Remnant Winter Water the primary source in the central region. In the slope region, the majority of nitrate changes at a given depth are due to the appearance of Atlantic Water in BC2. Changes within water masses are apparent at the interface above the Atlantic Water jet where an increase of 1–2 μM signals diapycnal nitrate flux. Offshore in the central region, much of the observed nitrate change is apparent as a change within water masses, for example, is likely due to mixing (Figure 6). In this region the Remnant Winter Water nitrate concentration decreased by 3 μM. The overlaying Bering Summer Water gained roughly the same amount of nitrate (Figure 6).

The observed nitrate changes can be compared with direct estimates of turbulent nitrate flux calculated from the microstructure sensors onboard the SuperSucker. Turbulent nitrate flux was calculated from the nitrate gradient and the GusT turbulent diffusivity estimates:

$$J_{NO_3} = K_T \frac{\partial NO_3}{\partial z}. \tag{6}$$

Following Hales et al. (2009), nutrient flux is only calculated where nutrient gradients are measurably large (for nitrate the threshold is $|\partial NO_3/\partial z| > 0.04\ \mu M\ m^{-1}$). This avoids large positive and negative flux values that occur in nearly well mixed layers in which the nutrient gradient is small but finite and poorly constrained while K_T is large due to the low stratification.

Turbulent nitrate flux values were as high as $\approx 4\ mmol\ m^{-2}\ day^{-1}$ (Figure 7). These observations are on the order of the maximum values found in the open Chukchi Sea during storm-driven mixing ($3.4\ mmol\ m^{-2}\ day^{-1}$Nishino et al., 2015). Similar levels of turbulent nitrate fluxes have been reported in other shallow regions in the Arctic (Bourgault et al., 2011; Randelhoff et al., 2016). Turbulent nitrate flux in the central Arctic are 2 orders of magnitude lower ($1.4 \times 10^{-2}\ mmol\ m^{-2}\ day^{-1}$; Randelhoff & Guthrie, 2016). The Barrow Canyon nitrate fluxes are comparable to values observed at some midlatitude shelf breaks (Hales et al., 2009), but less than those measured in a midlatitude coastal upwelling region

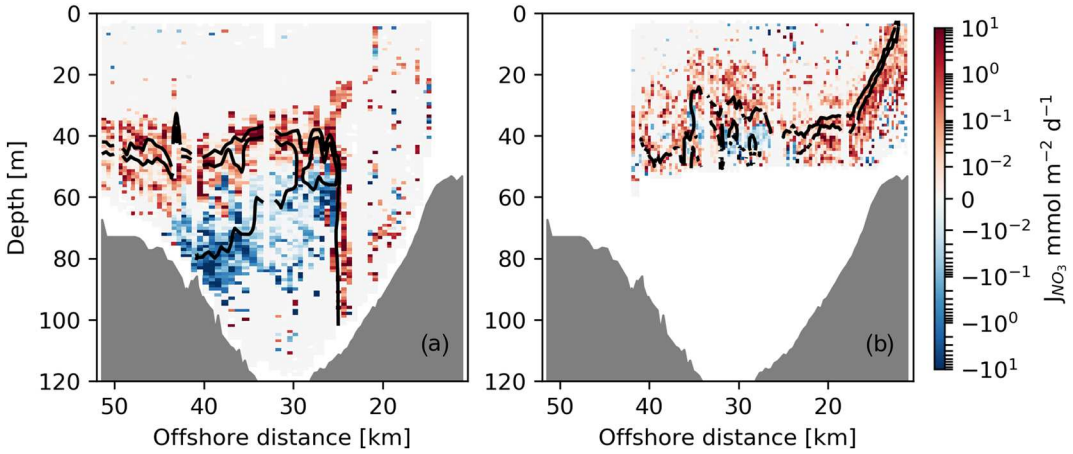

Figure 7. Vertical nitrate flux on BC1 (a) and BC2 (b). The 3 and 6 μM nitrate contours are shown for reference in black.

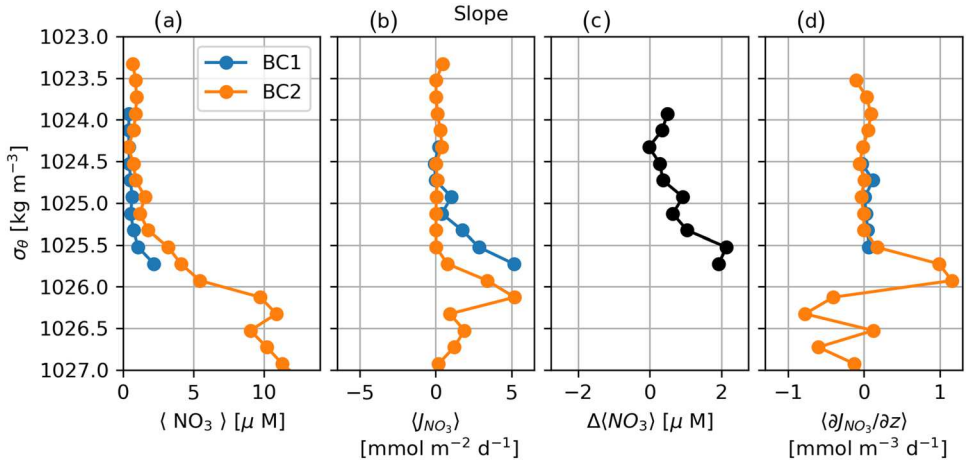

Figure 8. Slope region isopycnal averaged: nitrate (a), vertical nitrate flux (b), change in nitrate (c), and nitrate flux convergence (d).

(Hales, Moum, et al., 2005). As noted above, these turbulent fluxes are significantly smaller than the advective fluxes of the upwelling circulation. However, the turbulent flux represents an irreversible transfer of nitrate to lighter, shallower waters.

In the slope region, the area of upward (positive) nitrate flux increased significantly following upwelling when the Atlantic Water strengthened the vertical nitrate gradient (Figure 7). In the first Barrow Canyon occupation Alaskan Coastal Water above the onshore slope was largely depleted in nitrate, and much of the nitrate gradient in this region was below threshold for the flux calculation, except a region of high flux around 25 km offshore (Figure 7a). In the second occupation of slope, the nitrate gradient was large, and the vertical flux from the Atlantic Water into the layer above reached 4 mmol m^{-2} day^{-1} (Figure 7b).

Offshore, during the first occupation of the central region, strong positive and negative vertical nitrate gradients bounded the middepth nitrate maximum of the Remnant Winter Waters. The resulting turbulent fluxes are directed away from the nitrate maximum, upward above and downward below, the Remnant Winter Water layer (Figure 7a). This divergent turbulent flux acts to remove nitrate from the middepth maximum and transfer it to adjacent Bering Summer Water. During the second Barrow Canyon occupation, turbulent nitrate fluxes were mostly upward in the central canyon (Figure 7b). Small patches of downward flux created areas of divergence in the central canyon in BC2. These patches were coincident with the stirred region of high isopycnal temperature variance (Figure 3b). The temperature and salinity characteristics of the divergent patches suggest they are modified remains of Remnant Winter Water layer.

Above both the Atlantic and Remnant Winter Water, the turbulent nitrate flux reached similar values. The vertical advective nitrate flux associated with the Atlantic Water is much larger than turbulent flux from either water mass. However, when considering the importance of each of the two water mass contributions to the overall surface nitrate, we posit that the Remnant Winter Water is more prevalent in the region and thus is likely to be a larger integrated contributor over time.

Estimates of turbulent flux convergence can be compared with the changes observed in nitrate concentration. Because estimating flux convergence involves taking a vertical derivative of a noisy field like turbulent nitrate flux, some averaging must first be done to the flux observations. Rates of flux convergence were calculated in density space by averaging the flux estimates within isopycnal bins (bin size of 0.15 kg m^{-3}) and across each of the two regions. An estimate of the accumulation (or loss) of nitrate within an isopycnal layer is given by the convergence (divergence) of the averaged flux profile in density space times the average vertical density gradient (Figures 8 and 9):

$$\frac{\partial}{\partial z}J_{NO_3}=\frac{\partial}{\partial \rho}\langle J_{NO_3}\rangle\langle\frac{\partial \rho}{\partial z}\rangle=\frac{-\rho_o\langle N^2\rangle}{g}\frac{\partial}{\partial \rho}\langle J_{NO_3}\rangle, \tag{7}$$

where $\langle\cdot\rangle$ indicates averages in isopycnal bins across each region.

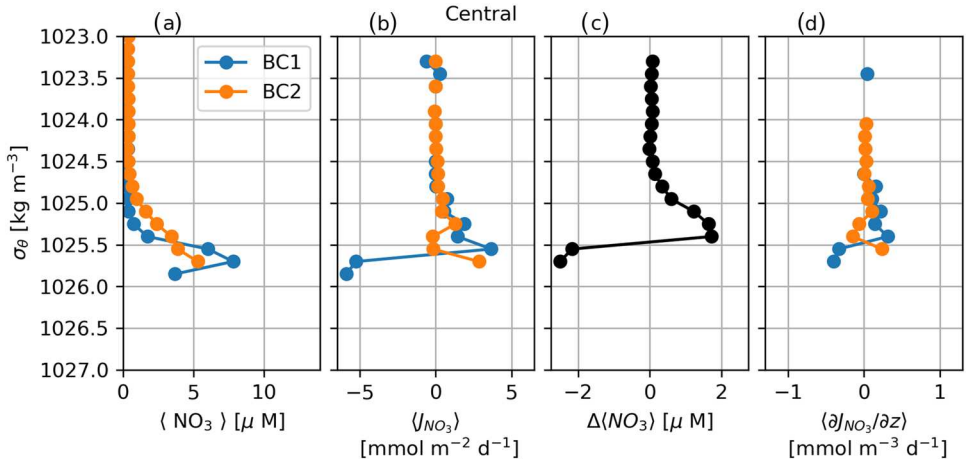

Figure 9. Central region isopycnal averaged: nitrate (a), vertical nitrate flux (b), change in nitrate (c), and nitrate flux convergence (d).

The nitrate flux convergence averaged over the slope region was small in the first occupation but increased dramatically to 1 mmol m^{-3} day^{-1} during BC2 (Figure 8d). The change in nitrate observed in the slope region (in the density range 1,024–1,025.7 kg m^{-3}; Figure 8c) is larger than what would be expected from the turbulent flux convergence calculated from BC1 or BC2 acting over the 6 days that elapsed between the two sections. It would take roughly 20 days, rather than six, for the observed turbulent flux convergence to result in the observed nitrate changes in that range; some additional unobserved mixing must be partially responsible for the increases in nitrate above the onshore canyon slope. It is possible that higher diffusivities earlier in the upwelling event increased the nitrate flux. Another possibility is the advection of waters from a higher flux region upcanyon of our section. Our two synoptic sections are unable to resolve the time or along-canyon evolution of the event.

Offshore of the canyon slope, away from the highly sheared jet, the observed nutrient changes and turbulent fluxes are more clearly balanced. The rate of the flux divergence from the Remnant Winter Water layer in the central canyon reached −0.3 mmol m^{-3} day^{-1} during BC1 (Figure 9d). Convergence in the layer of Bering Summer Water above was about equal and opposite at 0.26 mmol m^{-3} day^{-1}. The convergence and divergence estimates quantitatively show the transfer of nutrients from the Remnant Winter Water to adjacent water masses via turbulent flux. Given the observed change in nitrate in Figure 9c, the flux convergence in observed during BC1 could produce the observed changes in about 6–8 days. This timescale of turbulent flux is roughly the time separation between BC1 and BC2.

5.3. Biological Significance

Nitrate is a limiting nutrient in the Chukchi sea in late summer; thus, any physical process altering its distribution is likely to have an impact on biological production. While the upwelling event described here significantly alters the distribution of a limiting nutrient, an immediate biological response is not clear in our data. Changes in chlorophyll fluorescence and oxygen saturation in Barrow Canyon were largely consistent with the physical processes of advection and diffusion that impact the nitrate. Chlorophyll fluorescence is at a maximum at middepth, consistent with widely observed subsurface chlorophyll maxima in the area (Martini et al., 2016). There was some small change in chlorophyll fluorescence within water masses between the sections, but no significant increases in chlorophyll fluorescence were observed. Oxygen saturation also changed between BC1 and BC2 but appeared primarily to reflect mixing and advection rather than production. The observations are complicated by the timescale of biological response relative to our two synoptic sections. Thus, we find it challenging to isolate a biological response to the upwelling event from our synoptic data. However, we can comment on the potential biological significance of the observed nitrate advection and turbulent fluxes.

Turbulent nitrate fluxes reached 4 mmol m^{-2} day^{-1} in the central canyon and on the slope above the upwelled Atlantic Water. Using a Redfield ratio of C:N = 106:16, this flux is sufficient to support community production

rates of about 26 mmol C m^{-2} day^{-1}. These high rates are found both in the central canyon region above the Remnant Winter Water and on the canyon slope above the Atlantic Water. These observations show that both the Atlantic Water (upwelled in this case) and the Remnant Winter Water (which may be present more often) contribute to the nutrient flux. This is important to note given that Atlantic Water is not always advected to the head of the canyon (Weingartner et al., 2017); however, over the full length of the canyon nutrient rich Remnant Winter Waters are likely subject to similar dynamics and constitute an important source of nutrient flux. These direct observations of increased nutrient flux above particular water masses support previous work that found a strong correlation between phytoplankton biomass and deep nutrient-rich water masses (Lowry et al., 2015; Martini et al., 2016). The turbulent fluxes estimated here provide a physical mechanism to support these blooms above nutrient-rich water masses despite the strong stratification that characterizes the Chukchi shelf in late summer.

In addition to the turbulent fluxes, some fraction of the vertically advected nitrate flux may drive growth. A maximum estimate would assume that all the nitrate (70 mmol m^{-2} day^{-1}) was converted to carbon, supporting a growth rate of 463 mmol C m^{-2} day^{-1}. This rate seems unlikely, given that as of BC2 we did not see a significant increase in chlorophyll fluorescence within even the shallow Atlantic Water; however, this value provides an extreme upper bound on growth.

In addition to the potential size of the biological response to upwelling, our observations also suggest formation mechanisms for the small scales of observed phytoplankton patches. Our observations reveal spatially variable turbulent nitrate flux, and the production of patchy nutrient distributions via instability and stirring. These observations of patchy sources distributions of limiting nutrients may explain some of the scales of the subsurface chlorophyll maxima observed in the Chukchi Sea (Martini et al., 2016).

6. Conclusions

Here, we report on high-resolution observations of upwelling in Barrow Canyon. While nutrient upwelling in the region has been studied extensively, high-resolution physical and biogeochemical observations of these events have not been available. With our novel observations we quantify the advective and diapycnal fluxes of nitrate in Barrow Canyon. We also describe the property and stability characteristics of a dense gravity current formed by the nutrient-rich water upwelled from the Canada Basin.

Upwelling favorable winds blowing out of the northeast for 3 days reversed the circulation in Barrow Canyon and lifted nutrient-rich Atlantic Waters from the Canada Basin into the canyon. These nutrient-rich waters outcropped above the onshore slope of the canyon, where surface waters that had been depleted in nitrate were replaced by Atlantic Waters with nitrate concentrations as high as 14 μM. The event substantially altered the stratification, hydrographic properties, nutrient distribution, and circulation within Barrow Canyon.

After upwelling favorable wind forcing stopped, the raised waters adjusted to form a strongly sheared, highly baroclinic dense gravity current along the slope of the canyon. A secondary, frictional, transverse circulation developed within the gravity current that acted to connect the interior and interface of the dense jet. The potential vorticity structure of the current indicates that it was susceptible to multiple instabilities including quickly developing symmetric instability and more slowing growing baroclinic instability. These instabilities may be responsible for enhanced exchange of upwelled waters with nutrient-depleted waters offshore. Additionally, high wave number isopycnal temperature variance observed post upwelling suggests enhanced stirring of ambient water masses. This stirring may have been another consequence of instability.

The largest nitrate flux was due to advection, but significant turbulent fluxes were also found. Turbulent nitrate fluxes observed in the canyon (up to 4 mmol m^{-2} day^{-1}) are in the range of other high measurements in shallow regions around the Arctic, and midlatitude shelf break regions. Average turbulent flux divergences are found to be of the right order to explain changes in nitrate observed in the central canyon. Over the canyon slope, even though turbulent nitrate flux increased subsequent to upwelling, the estimated flux divergence is insufficient to produce the observed isopycnal nitrate changes.

These upwelling events can impact nutrient distributions in late summer when nutrients are depleted and may drive the growth rates and physical scales of phytoplankton biomass. While we are unable to isolate a biological response from our data, the turbulent fluxes measured would be sufficient to

support production of 26 mmol C m^{-2} day^{-1}. After the upwelling event, there is increased small-scale variability in the nitrate distribution that may play a role in the ubiquitous patchiness of the subsurface chlorophyll maxima in the region.

These unique observations illustrate the value of, and need for further, coordinated physical/biogeochemical observations of small-scale episodic events to understand their influence on the changing biogeochemistry of the Pacific Arctic. Such efforts would be timely given indications that upwelling events are becoming more common in the region.

Data Availability Statement

All data used in this work are freely available. HF radar data collected by the University of Alaska Fairbanks HF radar group are provided by the U.S. Integrated Ocean Observing System (IOOS) High Frequency Radar Network (HFRNet) and accessed through the Coastal Observing R&D Center (CORDC, https://cordc.ucsd.edu/projects/mapping/) THREDDS server (https://hfrnet-tds.ucsd.edu/thredds/catalog.html). Pt. Barrow meteorological data are available from the National Climate Data Center of the National Oceanic and Atmospheric Administration (http://www.ncdc.noaa.gov/). Shipboard ADCP and CTD data are available via the Rollingdeck to Repository (https://www.rvdata.us/search/cruise/SKQ201712SCruiseDOI:10.7284/907787). The in situ SuperSucker CTD and nutrient data from both Barrow Canyon sections used in the analysis are archived at the Arctic Data Center (doi:10.18739/A28S4JP6K) (Hales, 2020). Microstructure data processed to 1 s estimates of χ and ancillary variables from the gusT as well as SuperSucker-mounted ADCP shear are available the Arctic Data Center (doi:10.18739/A22F7JR7S) (Beaird & Shroyer, 2020).

Acknowledgments

We would like to thank the captain and crew of the R.V. *Sikuliaq*. We thank Dale Hubbard for SuperSucker operations. For help with the GusT we would like to thank Jim Moum, Pavan Vutukur, and Kerry Latham. We appreciate the efforts of the University of Alaska Fairbanks HF radar group for maintaining the HF radar surface current data in the region. Funding for this work was provided to Beaird and Shroyer by U.S. National Science Foundation (NSF) Arctic Natural Sciences Grant 1734777 and to Juranek, Hales, and Goñi by NSF Arctic Natural Sciences Grant 1504394. We would like to thank the communities responsible for the open source packages used for analysis and plotting including NumPy, SciPy, Pandas (pandas development team, 2020), Matplotlib (Hunter, 2007), and Xarray (Hoyer & Hamman, 2017; Hoyer et al., 2020). Additionally, we would like to thank three anonymous reviewers for their help in improving the manuscript.

References

Aagaard, K., & Roach, A. T. (1990). Arctic ocean-shelf exchange: Measurements in Barrow Canyon. *Journal of Geophysical Research*, *95*, 18,163–18,175. https://doi.org/10.1029/JC095iC10p18163

Arrigo, K. R. (2015). Impacts of Climate on EcoSystems and Chemistry of the Arctic Pacific Environment (ICESCAPE). *Deep Sea Research Part II: Topical Studies in Oceanography*, *118*, 1–6. https://doi.org/10.1016/j.dsr2.2015.06.007

Arrigo, K. R., & van Dijken, G. L. (2015). Continued increases in Arctic Ocean primary production. *Progress in Oceanography*, *136*, 60–70. https://doi.org/10.1016/j.pocean.2015.05.002

Arrigo, K. R., van Dijken, G., & Pabi, S. (2008). Impact of a shrinking Arctic ice cover on marine primary production. *Geophysical Research Letters*, *35*, L19603. https://doi.org/10.1029/2008GL035028

Ashjian, C. J., Braund, S. R., Campbell, R. G., George, J. C., Kruse, J., Maslowski, W., et al. (2010). Climate variability, oceanography, bowhead whale distribution, and Iñupiat subsistence whaling near Barrow, Alaska. *Arctic*, *63*, 179–194.

Batchelor, G. K. (1959). Small-scale variation of convected quantities like temperature in turbulent fluid Part 1. General discussion and the case of small conductivity. *Journal of Fluid Mechanics*, *5*(01), 113.

Beaird, N., & Shroyer, E. (2020). Physical impacts on late season productivity in changing Arctic, Chukchi Sea, 2017. Arctic Data Center. https://doi.org/10.18739/A22F7JR7S.

Bourgault, D., Hamel, C., Tremblay, J.-E., Galbraith, P. S., Dumont, D., & Gratton, Y. (2011). Turbulent nitrate fluxes in the Amundsen Gulf during ice-covered conditions. *Geophysical Research Letters*, *38*, L15602. https://doi.org/10.1029/2011GL047936

Bourke, R. H., & Paquette, R. G. (1976). Atlantic water on the Chukchi Shelf. *Geophysical Research Letters*, *3*(10), 629–632. https://doi.org/10.1029/GL003i010p00629

Brannigan, L. (2016). Intense submesoscale upwelling in anticyclonic eddies. *Geophysical Research Letters*, *43*, 3360–3369. https://doi.org/10.1002/2016GL067926

Codispoti, L. A., Kelly, V., Thessen, A., Matrai, P., Suttles, S., Hill, V., et al. (2013). Synthesis of primary production in the Arctic Ocean: III. Nitrate and phosphate based estimates of net community production. *Progress in Oceanography*, *110*, 126–150.

Comiso, J. C. (2012). Large decadal decline of the Arctic multiyear ice cover. *Journal of Climate*, *25*(4), 1176–1193.

Corlett, W. B., & Pickart, R. S. (2017). The Chukchi slope current. *Progress in Oceanography*, *153*, 50–65.

D'Asaro, E. A. (1988). Generation of submesoscale vortices: A new mechanism. *Journal of Geophysical Research*, *93*(C6), 6685.

Darelius, E. (2008). Topographic steering of dense overflows: Laboratory experiments with V-shaped ridges and canyons. *Deep Sea Research Part I: Oceanographic Research Papers*, *55*(8), 1021–1034.

Fang, Y.-C., Potter, R. A., Statscewich, H., Weingartner, T. J., Winsor, P., & Irving, B. K. (2017). Surface current patterns in the northeastern Chukchi Sea and their response to wind forcing. *Journal of Geophysical Research: Oceans*, *122*, 9530–9547. https://doi.org/10.1002/2017JC013121

Fer, I., Voet, G., Seim, K. S., Rudels, B., & Latarius, K. (2010). Intense mixing of the Faroe Bank Channel overflow. *Geophysical Research Letters*, *37*, L02604. https://doi.org/10.1029/2009GL041924

Fischer, J., & Visbeck, M. (1993). Deep velocity profiling with self-contained ADCPs. *Journal of Atmospheric and Oceanic Technology*, *10*(5), 764–773.

Garvine, R. W. (1971). A simple model of coastal upwelling dynamics. *Journal of Physical Oceanography*, *1*(3), 169–179.

Grebmeier, J. M., Cooper, L. W., Feder, H. M., & Sirenko, B. I. (2006). Ecosystem dynamics of the Pacific-influenced Northern Bering and Chukchi Seas in the Amerasian Arctic. *Progress in Oceanography*, *71*(2-4), 331–361. https://doi.org/10.1016/j.pocean.2006.10.001

Grebmeier, J. M., Overland, J. E., Moore, S. E., Farley, E. V., Carmack, E., Cooper, L. W., et al. (2006). A major ecosystem shift in the northern Bering Sea. *Science*, *311*(5766), 1461–1464. https://doi.org/10.1126/science.1121365

Gregg, M. C., D'Asaro, E. A., Riley, J. J., & Kunze, E. (2018). Mixing efficiency in the ocean. *Annual Review of Marine Science*, *10*, 443–473.

Hales, B. (2020). Ocean nutrient and chemistry data collected using the supersucker from the Chuchki Sea, 2016–2017. Arctic Data Center. doi:10.18739/A28S4JP6K.
Hales, B., Hebert, D., & Marra, J. (2009). Turbulent supply of nutrients to phytoplankton at the New England shelf break front. *Journal of Geophysical Research*, *114*, C05010. https://doi.org/10.1029/2008JC005011
Hales, B., Moum, J. N., Covert, P., & Perlin, A. (2005). Irreversible nitrate fluxes due to turbulent mixing in a coastal upwelling system. *Journal of Geophysical Research*, *110*, C10S11. https://doi.org/10.1029/2004JC002685
Hales, B., Takahashi, T., & Bandstra, L. (2005). Atmospheric CO_2 uptake by a coastal upwelling system. *Global Biogeochemical Cycles*, *19*, GB1009. https://doi.org/10.1029/2004GB002295
Hoskins, B. J. (1974). The role of potential vorticity in symmetric stability and instability. *Quarterly Journal of the Royal Meteorological Society*, *100*(425), 480–482.
Hoyer, S., & Hamman, J. (2017). xarray: ND labeled arrays and datasets in Python. *Journal of Open Research Software*, *5*, 1–10. http://doi.org/10.5334/jors.148
Hoyer, S., Hamman, J., Roos, M., Cherian, D., Fitzgerald, C., Fujii, K., et al. (2020). pydata/xarray: v0.15.1. https://doi.org/10.5281/zenodo.3724893
Hunter, J. D. (2007). Matplotlib: A 2D graphics environment. *Computing in Science & Engineering*, *9*(3), 90–95. https://doi.org/10.1109/MCSE.2007.55
Johnson, G. C., & Ohlsen, D. R. (1994). Frictionally modified rotating hydraulic channel exchange and ocean outflows. *Journal of Physical Oceanography*, *24*(1), 66–78.
Kahru, M., Lee, Z., Mitchell, B. G., & Nevison, C. D. (2016). Effects of sea ice cover on satellite-detected primary production in the Arctic Ocean. *Biology Letters*, *12*(11), 1–5. https://doi.org/10.1098/rsbl.2016.0223
Ladd, C., Mordy, C. W., Salo, S. A., & Stabeno, P. J. (2016). Winter water properties and the Chukchi Polynya. *Journal of Geophysical Research: Oceans*, *121*, 5516–5534. https://doi.org/10.1002/2016JC011918
Li, M., Pickart, R. S., Spall, M. A., Weingartner, T. J., Lin, P., Moore, G. W. K., & Qi, Y. (2019). Circulation of the Chukchi Sea shelfbreak and slope from moored timeseries. *Progress in Oceanography*, *172*, 14–33.
Lin, P., Pickart, R. S., McRaven, L. T., Arrigo, K. R., Bahr, F., Lowry, K. E., et al. (2019). Water mass evolution and circulation of the northeastern Chukchi Sea in summer: Implications for nutrient distributions. *Journal of Geophysical Research: Oceans*, *124*, 4416–4432. https://doi.org/10.1029/2019JC015185
Lin, P., Pickart, R. S., Moore, G. W. K., Spall, M. A., & Hu, J. (2019). Characteristics and dynamics of wind-driven upwelling in the Alaskan Beaufort Sea based on six years of mooring data. *Deep Sea Research Part II: Topical Studies in Oceanography*, *162*, 79–92.
Lin, P., Pickart, R. S., Stafford, K. M., Moore, G. W. K., Torres, D. J., Bahr, F., & Hu, J. (2016). Seasonal variation of the Beaufort shelfbreak jet and its relationship to Arctic cetacean occurrence. *Journal of Geophysical Research: Oceans*, *121*, 8434–8454. https://doi.org/10.1002/2016JC011890
Lowry, K. E., Pickart, R. S., Mills, M. M., Brown, Z. W., van Dijken, G. L., Bates, N. R., & Arrigo, K. R. (2015). The influence of winter water on phytoplankton blooms in the Chukchi Sea. *Deep Sea Research Part II: Topical Studies in Oceanography*, *118*, 53–72.
Mahadevan, A. (2016). The impact of submesoscale physics on primary productivity of plankton. *Annual Review of Marine Science*, *8*(1), 161–184. https://doi.org/10.1146/annurev-marine-010814-015912
Martini, K. I., Stabeno, P. J., Ladd, C., Winsor, P., Weingartner, T. J., Mordy, C. W., & Eisner, L. B. (2016). Dependence of subsurface chlorophyll on seasonal water masses in the Chukchi Sea. *Journal of Geophysical Research: Oceans*, *121*, 1755–1770. https://doi.org/10.1002/2015JC011359
Maslanik, J., Stroeve, J., Fowler, C., & Emery, W. (2011). Distribution and trends in Arctic sea ice age through spring 2011. *Geophysical Research Letters*, *38*, L13502. https://doi.org/10.1029/2011GL047735
Mathis, J. T., Pickart, R. S., Byrne, R. H., McNeil, C. L., Moore, G. W. K., Juranek, L. W., et al. (2012). Storm-induced upwelling of high p CO_2 waters onto the continental shelf of the western Arctic Ocean and implications for carbonate mineral saturation states. *Geophysical Research Letters*, *39*, L07606. https://doi.org/10.1029/2012GL051574
Moore, S. E., & Grebmeier, J. M. (2018). The distributed biological observatory: Linking physics to biology in the Pacific Arctic region+ supplementary file (see article tools). *Arctic*, *71*(5), 1–7.
Moum, J. N. (2015). Ocean speed and turbulence measurements using pitot-static tubes on moorings. *Journal of Atmospheric and Oceanic Technology*, *32*(7), 1400–1413.
Moum, J. N., & Nash, J. D. (2009). Mixing measurements on an equatorial ocean mooring. *Journal of Atmospheric and Oceanic Technology*, *26*(2), 317–336. https://doi.org/10.1175/2008JTECHO617.1
Naveira-Garabato, A. C., Frajka-Williams, E. E., Spingys, C. P., Legg, S., Polzin, K. L., Forryan, A., et al. (2019). Rapid mixing and exchange of deep-ocean waters in an abyssal boundary current. *Proceedings of the National Academy of Sciences*, *116*(27), 13,233–13,238. https://doi.org/10.1073/pnas.1904087116
Nishino, S., Kawaguchi, Y., Inoue, J., Hirawake, T., Fujiwara, A., Futsuki, R., et al. (2015). Nutrient supply and biological response to wind-induced mixing, inertial motion, internal waves, and currents in the northern Chukchi Sea. *Journal of Geophysical Research: Oceans*, *120*, 1975–1992. https://doi.org/10.1002/2014JC010407
Osborn, T. R. (1980). Estimates of the local rate of vertical diffusion from dissipation measurements. *Journal of Physical Oceanography*, *10*, 83–89.
Osborn, T. R., & Cox, C. S. (1972). Oceanic fine structure. *Geophysical Fluid Dynamics*, *3*(1), 321–345. https://doi.org/10.1080/03091927208236085
pandas development team, T. (2020). pandas-dev/pandas: Pandas. https://doi.org/10.5281/zenodo.3509134
Pickart, R. S. (2004). Shelfbreak circulation in the Alaskan Beaufort Sea: Mean structure and variability. *Journal of Geophysical Research*, *109*, C04024. https://doi.org/10.1029/2003JC001912
Pickart, R. S., Nobre, C., P., L., Arrigo, K. R., Ashjian, C. J., Berchok, C., et al. (2019). Seasonal to mesoscale variability of water masses and atmospheric conditions in Barrow Canyon, Chukchi Sea. *Deep Sea Research Part II: Topical Studies in Oceanography*, *162*, 32–49.
Pickart, R. S., Schulze, L. M., Moore, G. W. K., Charette, M. A., Arrigo, K. R., van Dijken, G., & Danielson, S. L. (2013). Long-term trends of upwelling and impacts on primary productivity in the Alaskan Beaufort Sea. *Deep-Sea Research I*, *79*, 106–121.
Pickart, R. S., Spall, M. A., & Mathis, J. T. (2013). Dynamics of upwelling in the alaskan beaufort sea and associated shelf-basin fluxes. *Deep-Sea Research I*, *76*, 35–51.
Pickart, R. S., Spall, M. A., Moore, G. W. K., Weingartner, T. J., Woodgate, R. A., Aagaard, K., & Shimada, K. (2011). Upwelling in the Alaskan Beaufort Sea: Atmospheric forcing and local versus non-local response. *Progress in Oceanography*, *88*(1-4), 78–100. https://doi.org/10.1016/j.pocean.2010.11.005

Pisareva, M. N., Pickart, R. S., Fratantoni, P. S., & Weingartner, T. J. (2019). On the nature of wind-forced upwelling in Barrow Canyon. *Deep Sea Research Part II: Topical Studies in Oceanography*, *162*, 63–78.
Randelhoff, A., Fer, I., Sundfjord, A., Tremblay, J.-E., & Reigstad, M. (2016). Vertical fluxes of nitrate in the seasonal nitracline of the Atlantic sector of the Arctic Ocean. *Journal of Geophysical Research: Oceans*, *121*, 5282–5295. https://doi.org/10.1002/2016JC011779
Randelhoff, A., & Guthrie, J. D. (2016). Regional patterns in current and future export production in the central Arctic Ocean quantified from nitrate fluxes. *Geophysical Research Letters*, *43*, 8600–8608. https://doi.org/10.1002/2016GL070252
Schulze, L. M., & Pickart, R. S. (2012). Seasonal variation of upwelling in the Alaskan Beaufort Sea: Impact of sea ice cover. *Journal of Geophysical Research*, *117*, C06022. https://doi.org/10.1029/2012JC007985
Shroyer, E. L. (2012). Turbulent kinetic energy dissipation in Barrow Canyon. *Journal of Physical Oceanography*, *42*(6), 1012–1021. https://doi.org/10.1175/JPO-D-11-0184.1
Signorini, S. R., Münchow, A., & Haidvogel, D. (1997). Flow dynamics of a wide Arctic canyon. *Journal of Geophysical Research*, *102*(C8), 18,661–18,680. https://doi.org/10.1029/97JC00739
Smith, D. M. (1998). Recent increase in the length of the melt season of perennial Arctic sea ice. *Geophysical Research Letters*, *25*(5), 655–658. https://doi.org/10.1029/98GL00251
Taylor, G. I. (1935). Statistical theory of turbulence. *Proceedings of the Royal Society of London*, *151*, 421–454.
Thomas, L. N., Tandon, A., & Mahadevan, A. (2008). Submesoscale processes and dynamics. *Ocean Modeling in an Eddying Regime*, *177*, 17–38.
Thomas, L. N., Taylor, J. R., Ferrari, R., & Joyce, T. M. (2013). Symmetric instability in the Gulf Stream. *Deep Sea Research Part II: Topical Studies in Oceanography*, *91*, 96–110. https://doi.org/10.1016/j.dsr2.2013.02.025
Thurnherr, A. M. (2011). Vertical velocity from ladcp data. In *2011 ieee/oes 10th current, waves and turbulence measurements (cwtm)*, IEEE, pp. 198–204.
Timmermans, M.-L., & Winsor, P. (2013). Scales of horizontal density structure in the Chukchi Sea surface layer. *Continental Shelf Research*, *52*, 39–45. https://doi.org/10.1016/j.csr.2012.10.015
Umlauf, L., & Arneborg, L. (2009). Dynamics of rotating shallow gravity currents passing through a channel. Part I: Observation of transverse structure. *Journal of Physical Oceanography*, *39*(10), 2385–2401.
Umlauf, L., Arneborg, L., Hofmeister, R., & Burchard, H. (2010). Entrainment in shallow rotating gravity currents: A modeling study. *Journal of Physical Oceanography*, *40*(8), 1819–1834. https://doi.org/10.1175/2010JPO4367.1
Wåhlin, A. K. (2004). Downward channeling of dense water in topographic corrugations. *Deep Sea Research Part I: Oceanographic Research Papers*, *51*(4), 577–590.
Weingartner, T., Aagaard, K., Woodgate, R., Danielson, S., Sasaki, Y., & Cavalieri, D. (2005). Circulation on the north central Chukchi Sea shelf. *Deep Sea Research Part II: Topical Studies in Oceanography*, *52*(24-26), 3150–3174. https://doi.org/10.1016/j.dsr2.2005.10.015
Weingartner, T. J., Cavalieri, D. J., Aagaard, K., & Sasaki, Y. (1998). Circulation, dense water formation, and outflow on the northeast Chukchi Shelf. *Journal of Geophysical Research*, *103*(C4), 7647–7661. https://doi.org/10.1029/98JC00374
Weingartner, T., Dobbins, E., Danielson, S., Winsor, P., Potter, R., & Statscewich, H. (2013). Hydrographic variability over the northeastern Chukchi Sea shelf in summer-fall 2008–2010. *Continental Shelf Research*, *67*, 5–22. https://doi.org/10.1016/j.csr.2013.03.012
Weingartner, T. J., Potter, R. A., Stoudt, C. A., Dobbins, E. L., Statscewich, H., Winsor, P. R., et al. (2017). Transport and thermohaline variability in Barrow Canyon on the Northeastern Chukchi Sea Shelf. *Journal of Geophysical Research*, *122*, 3565–3585. https://doi.org/10.1002/2016JC012636
Wenegrat, J. O., & Thomas, L. N. (2020). Centrifugal and symmetric instability during Ekman adjustment of the bottom boundary layer. *Journal of Physical Oceanography*, *50*(6), 1793–1812.
Woodgate, R. A., Aagaard, K., & Weingartner, T. J. (2005). A year in the physical oceanography of the Chukchi Sea: Moored measurements from autumn 1990–1991. *Deep-Sea Research Part II*, *52*, 3116–3149.